THREE-DIMENSIONAL SIMULATIONS OF LEAN H_2-AIR FLAMES PROPAGATING IN A NARROW GAP: ON THE VALIDITY OF THE QUASI-TWO-DIMENSIONAL APPROXIMATION

J. Melguizo-Gavilanes[1], D. Fernández-Galisteo[2], A. Dejoan[2], M. Sánchez-Sanz[3], V. N. Kurdyumov[2]

[1]**Institute Pprime, UPR 3346 CNRS, ISAE-ENSMA, 86961, Futuroscope-Chasseneuil, France**

[2]**Department of Energy, CIEMAT, Avenida Complutense 40, 28040, Madrid, Spain**

[3]**Departmento de Ingeniería Térmica y de Fluidos, Universidad Carlos III de Madrid, 28911, Leganés, Spain**

Abstract

The premixed propagation of lean isobaric H_2-air flames ($\phi = 0.3$) in Hele-Shaw cells (i.e. two parallel plates separated by a small distance, h, on the order of the thickness of the planar adiabatic flame, $\delta_f \sim 3$ mm) is investigated numerically. Three-dimensional (3D) simulations with detailed chemistry and transport are used to examine the effect of h on the flame dynamics and its overall normalized propagation speed (S_T/S_L) for a semi-closed system of size $25\delta_f \times 25\delta_f \times h$. To determine the validity of an existing quasi-two-dimensional (quasi-2D) formulation (derived in the limit of $h \to 0$) to capture the 3D dynamics, results for $h = 0.1\delta_f$, $h = 0.5\delta_f$, and $h = \delta_f$ are reported. For $h = 0.1\delta_f$ strong cell splitting/merging is observed with associated low frequency/high amplitude oscillations in the temporal evolution of S_T/S_L (10-17Hz; $6 \leq S_T/S_L \leq 10$). Larger values of h exhibit a much smoother evolution. For $h = 0.5\delta_f$ the cell splitting/merging is milder relaxing to a steady propagating speed of $S_T/S_L \sim 6$ after an initial transient; for $h = 1\delta_f$, the flame dynamics along the h direction starts to play an important role showing two distinct phases: (i) initial symmetric propagation with a linear increase in S_T/S_L (from 5.3 to 6.8) as early signs of asymmetry are visible, (ii) followed by a fully non-symmetric propagation resulting in an abrupt increase in S_T/S_L that quickly relaxes to a constant value thereafter ($S_T/S_L \sim 10$). Our preliminary results suggest that for the lean H_2-air mixture considered the quasi-2D approximation breaks down for $h > 0.1\delta_f$.

NOMENCLATURE

Symbol	Definition
a	h/δ_f
$\mathcal{D}^T$	Thermal Diffusion
$\mathcal{D}_m$	Mass diffusivity
h	Separation distance between plates
h_s	Mixture sensible enthalpy
$\mathbf{j_k}$	Mass flux vector
$\mathbf{j_q}$	Heat flux vector
L_x, L_y	Horizontal and vertical Hele-Shaw lengths
N_{max}	Number of cells in grid
$\mathcal{N}$	Total number of chemical species
p	Gas pressure
$\mathcal{R}$	Universal gas constant
r_{ign}	Ignition radius
S_L	Laminar burning velocity
S_T	Integrated consumption rate
T	Gas temperature
t	Time
$\mathbf{u}$	Gas velocity vector
W	Molecular weight
$\overline{W}$	Mixture Molecular weight
Y	Mass fraction

Subindices	
ad	Adiabatic
b	Burned
f	Flame
k	kth species
u	Unburned

Greek letters	
δ_f	Thickness of the planar flame
μ	Gas viscosity
ρ	Gas density
τ	Stress Tensor
ϕ	Equivalence ratio

1. INTRODUCTION

The study of flames in confined geometries is relevant to the development of combustors and internal combustion engines, as well as to provide further insight on safety issues and undesired propagation of confined reactions in small channels, gaps and tubes. In turn, micro-combustion devices have benefited from the study of flame instabilities [1–4], thermoacoustic coupling [5], flame extinction and quenching [6], among others. The analysis of premixed flames in narrow gaps is key to understanding most of these phenomena, typically enhanced by the geometrical constraint of the flow. Experimental, theoretical and numerical efforts have given valuable insight on the flame topology, the propagation rate and the flame stability under various conditions and regimes [7–11].

Safety issues related to fuel leaks that may lead to accidental fires and explosions motivate the study of lean flame propagation from a fundamental point of view. Besides the most destructive events, such as detonations and material combustion, one of the current challenges is the detection and control of very lean and slow-burning combustion fronts with very weak pressure rise [12] that can bring undesired hot spots into flammable regions [13].

Recent research used the quasi-2D approximation to computationally study the propagation of premixed flames in slender, 3D Hele-Shaw cells, with comparable size for the longitudinal, L_x, and transverse, L_y, lengths ($L_y \sim L_x$) which are much larger than the distance, h, that separates the parallel plates ($h \ll L_x$) [9, 11, 14]. This approximation takes the limit $h/\delta_f \ll 1$, with δ_f being the thermal flame thickness, to asymptotically reduce the 3D character of the problem to a quasi-2D approximation in

which the velocity field reduces to a Poiseuille parabolic profile, and both temperature and mass fraction of chemical species are uniform along the transverse direction, h. Nevertheless, the experimental measurements published by Veiga et al. [10, 13, 15] and Martínez et al. [16] clearly identified a curved reaction front along h that questions the main hypothesis of the narrow channel approximation which is used to reduce the computational cost. The goal of this study is thus to precisely determine to what extent the aforementioned approximation is valid.

2. COMPUTATIONAL METHODOLOGY

2.1. Governing equations, transport and chemical model

In the 3D simulations, the dynamics of the flame front is determined by solving the low Mach number, variable-density, reactive Navier-Stokes equations with detailed chemistry and transport [17]:

$$\frac{\partial \rho}{\partial t} + \nabla\cdot(\rho\mathbf{u}) = 0, \tag{1}$$

$$\frac{\partial}{\partial t}(\rho\mathbf{u}) + \nabla\cdot(\rho\mathbf{u}\cdot\mathbf{u}) = -\nabla p + \nabla\cdot\tau, \tag{2}$$

$$\frac{\partial}{\partial t}(\rho Y_k) + \nabla\cdot(\rho\mathbf{u}Y_k) = -\nabla\cdot\mathbf{j}_\mathrm{k} + \dot{\omega}_k, \tag{3}$$

$$\frac{\partial}{\partial t}(\rho h_s) + \nabla\cdot(\rho\mathbf{u}h_s) = -\nabla\cdot\mathbf{j}_\mathrm{q} - \sum_{k=1}^{\mathcal{N}}\Delta h^0_{f_k}\,\dot{\omega}_k, \tag{4}$$

with the ideal gas equation of state and deviatoric stress tensor given by:

$$p = \rho\frac{\mathcal{R}}{\overline{W}}T \text{ with } \overline{W} = 1/\sum_{k}^{\mathcal{N}}(Y_k/W_k); \quad \tau = \mu(\nabla\mathbf{u} + \nabla\mathbf{u}^T) - \frac{2}{3}\mu(\nabla\cdot\mathbf{u})\mathbf{I} \tag{5}$$

The mass flux and the heat flux have the form $\mathbf{j}_\mathrm{k} = -\rho\,\mathcal{D}_{k,m}\nabla Y_k - \mathcal{D}^T_k\nabla T/T$ and $\mathbf{j}_\mathrm{q} = -\lambda/c_p\,(\nabla h_s - \sum_{k=1}^{\mathcal{N}} h_{s_k}\nabla Y_k) + \sum_{k=1}^{\mathcal{N}}\mathbf{j}_\mathrm{k}h_{s_k}$, respectively. The governing equations (1)-(5) were solved using the Open source Field Operation And Manipulation (OpenFOAM) toolbox [18]. The base implementation of the code is well validated as it has been successfully used in various studies performed by the first author of the current study, ranging from thermal ignition to lean hydrogen flame dynamics, comprising different geometries, modes of heat transfer (e.g. forced and natural convection), and ignition timescales [12, 19–23]; for details on the numerical methods used see [21]. Two major improvements over the base implementation included in this study are: (i) a Cantera [24] class to accurately determine the mixture viscosity/thermal conductivity, and mass diffusivities of individual species into the mixture, including thermodiffusion (Soret effect); (ii) an Adaptive Mesh Refinement (AMR) capability to tackle 3D problems in a computationally efficient manner. The standard OpenFOAM libraries are used for the latter. The chemistry was modeled using Mével's mechanism for hydrogen oxidation which includes $\mathcal{N} = 9$ species and 21 reactions [25, 26]. This mechanism has been extensively validated, and reproduces flame speeds and ignition delay times to a reasonable degree of accuracy over a wide range of concentrations.

In the quasi-2D formulation, the full set of equations (1)-(5) should be recast by taking the asymptotic limit $h/\delta_f \ll 1$. The resulting set of equations is governed by Darcy's law, that relates the average velocity and the pressure fields through the following relation:

$$\mathbf{u} = -\frac{h^2}{12\mu}\nabla p, \tag{6}$$

In (6) the operator ∇ and the velocity field $\mathbf{u}$ are defined only in the xy-plane (see Fig. 1). Equation (2) should then be replaced by (6) and both temperature and mass fractions become uniform in transverse direction L_z when the walls bounding the flow at $L_{z,\min} = 0$ and $L_{z,\max} = h$ are assumed to be adiabatic [14]. While in the present work, we only qualitatively compare the full 3D flame dynamics with the quasi-2D (dimensionless) analysis published earlier by [9, 14], we deemed necessary to describe briefly the main assumptions made.

2.2. Domain, initial and boundary conditions

The computational domain is an adiabatic 3D cell with dimensions $L_x = L_y = 25\delta_f$, and variable distance between the plates $L_z = h$ (see Fig. 1).

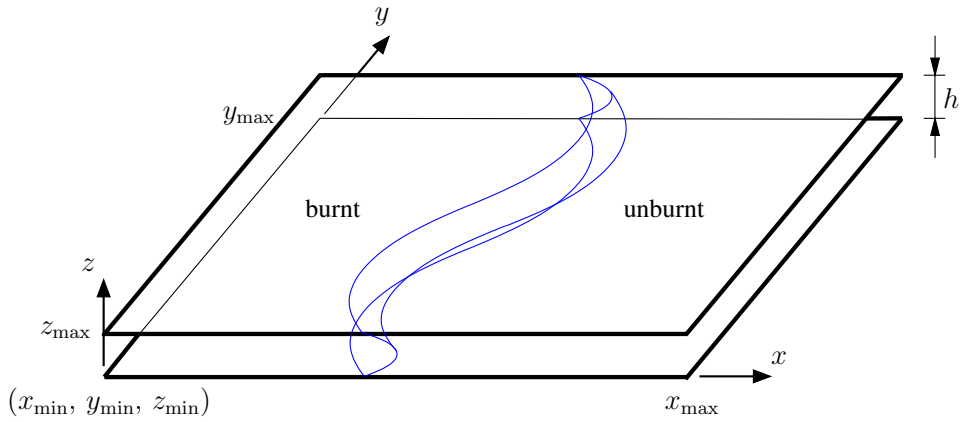

Figure 1: Schematic representation of the Hele-Shaw cell with a curved flame propagating from left to right showing the distance between the plates h. Adapted from [9].

Three cases are considered $h = 0.1\delta_f$, $0.5\delta_f$ and δ_f, where the thermal flame thickness, $\delta_f = (T_{\text{ad}} - T_u)/(dT/dx)_{\max}$, is computed using the one-dimensinoal (1D) steady planar flame profiles obtained with Cantera. T_{ad} and $(dT/dx)_{\max}$ are the adiabatic flame temperature and maximum spatial temperature gradient, respectively. The channel is initialy filled with a quiescent, lean H_2-air mixture ($\phi = 0.3$) at ambient temperature and pressure characterized by $Y_{u,H_2} = 0.008727$, $Y_{u,O_2} = 0.230885$, $Y_{u,N_2} = 0.760388$, $p_u = 100$ kPa, $T_u = 300$ K and $\mathbf{u} = (0, 0, 0)$, whose laminar flame properties are $S_L = 0.0309$ m/s, $T_{\text{ad}} = 1173.4$ K and $\delta_f = 2.75$ mm. The mixture is numerically ignited using five hemicylindrical regions of radius $r_{\text{ign}} = 4\delta_f$ located at $x/\delta_f = 0$ and $y/\delta_f = 0.0, 6.25, 12.5, 18.75, 25$ filled with its corresponding equilibrium composition (T_{ad} and $Y_{i,\text{eq}}$) determined with Cantera. The flame propagates from left (open end) to right (closed end) confined by two parallel plates along the L_z-direction. As shown in [10], the residence time of the acoustic wave $t_a \sim 2L_x/c$, with $c \simeq 688$ m/s at chemical equilibrium, is much longer than the acoustic dissipation time $t_d \sim \rho h^2/\mu$ and the interaction between flame and acoustics can be neglected. The boundary conditions on walls ($L_x = x_{\max}$, $L_z = z_{\min}$ and $L_z = z_{\max}$) are no-slip for velocity and zero gradient for all scalar variables, whereas at $L_y = y_{\min}$ and $L_y = y_{\max}$ periodicity is imposed to mimic an infinitely long physical domain in that direction. Note that ignition regions at $y/\delta_f = 0$ and $y/\delta_f = 25$ are thus part of the same periodic condition. At the open end, $L_x = x_{\min}$, the pressure is fixed and equal to atmospheric pressure; a zero gradient condition is applied for velocity and scalar variables. Finally, the initial mesh is chosen to have 4 points per δ_f on the xy-plane ($\Delta x = \Delta y = \delta_f/4$) and $\Delta z = h/4$ on the xz-plane. The mesh refinement metric used is the normalized temperature gradient field, computed at each time step, which ensures an effective local resolution of 20 points per δ_f even fior highly curved flames. Two refinement levels are used, and the maximum number of cells allowed in the domain, $N_{\max}$, is restricted to 1 million, however for the cases

considered $N_{\max} \sim 200$k (at least 5 times smaller than the resolution required on a fixed mesh). The computational cost per case was 3920 CPU hours.

3. RESULTS AND DISCUSSION

Figure 2 shows the time history of the normalized integrated consumption rate

$$\frac{S_T}{S_L} = \frac{1}{\rho_u Y_{\mathrm{H_{2_u}}} L_y h S_L} \iiint_V \dot{\omega}_{\mathrm{H_2}} \mathrm{d}V$$

recorded at each time speed during the simulation for all values of h considered.

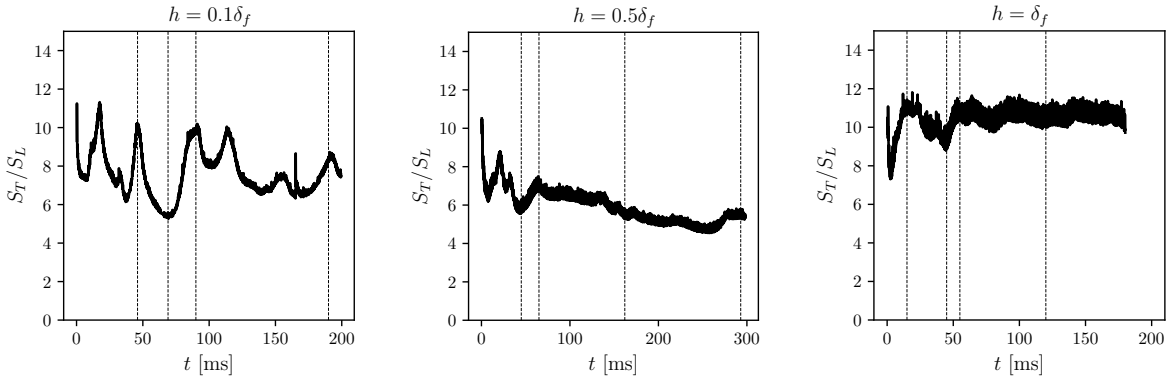

Figure 2: Time history of normalized consumption rate, S_T/S_L, for $h = 0.1\delta_f$, $0.5\delta_f$ and δ_f. Dashed vertical lines are visual indicators showing the times at which field measurements are taken.

The S_T/S_L shows a clear influence of h on the flame dynamics. For $h = 0.1\delta_f$ low frequency/high amplitude oscillations of 10-17 Hz and $5 \leq S_T/S_L \leq 11$, are visible and likely related to cell splitting/merging; the latter oscillatory behavior was also reported using the quasi-2D approximation [9]. An increase in the distance between plates to $h = 0.5\delta_f$ results in a similar S_T/S_L history to $h = 0.1\delta_f$ for $t \leq 45$ ms, albeit smaller amplitudes, followed by a very long linearly decreasing transient in normalized consumption rate ($65 \leq t \leq 260$ ms). Shortly before reaching the end wall, the flame propagates steadily at $S_T/S_L \sim 5.5 - 6$. Finally, for $h = \delta_f$, after an initial transient, the S_T/S_L records quickly converge to a steady propagation speed of $S_T/S_L \sim 10$ for $t \geq 55$ ms. The average consumption rates computed from the time histories presented in Fig. 2 are 7.78, 5.95 and 10.09 for increasing h, which suggests a non-linear dependence of S_T/S_L on the separation distance h. The temperature fields presented in Figs. 3 to 5 will shed light on the differences observed.

Figure 3 shows representative flame topologies associated to local maxima ($t = 46$, 90 and 190 ms) and the global minimum ($t = 69$ ms) observed during propagation for $h = 0.1\delta_f$ (see dashed lines in Fig. 2). Note that the temperature fields are uniform at all times in the $z-$direction, suggesting that the quasi-2D approximation holds. In the xy-plane strong cells splitting/merging is present. Peaks in S_T/S_L are correlated with the occurrence of cell merging (after which the flame surface area decreases) whereas troughs are associated to cell splitting (after which the flame surface area increases). The dynamics of propagation during the time frame considered is rather rich showing an initial transient where the characteristic size of the cells is evenly distributed/symmetric ranging between $2.5 - 5\delta_f$ ($t = 46 - 90$ ms); at later times ($t = 190$ ms) strong confinement, and the proximity to the end wall

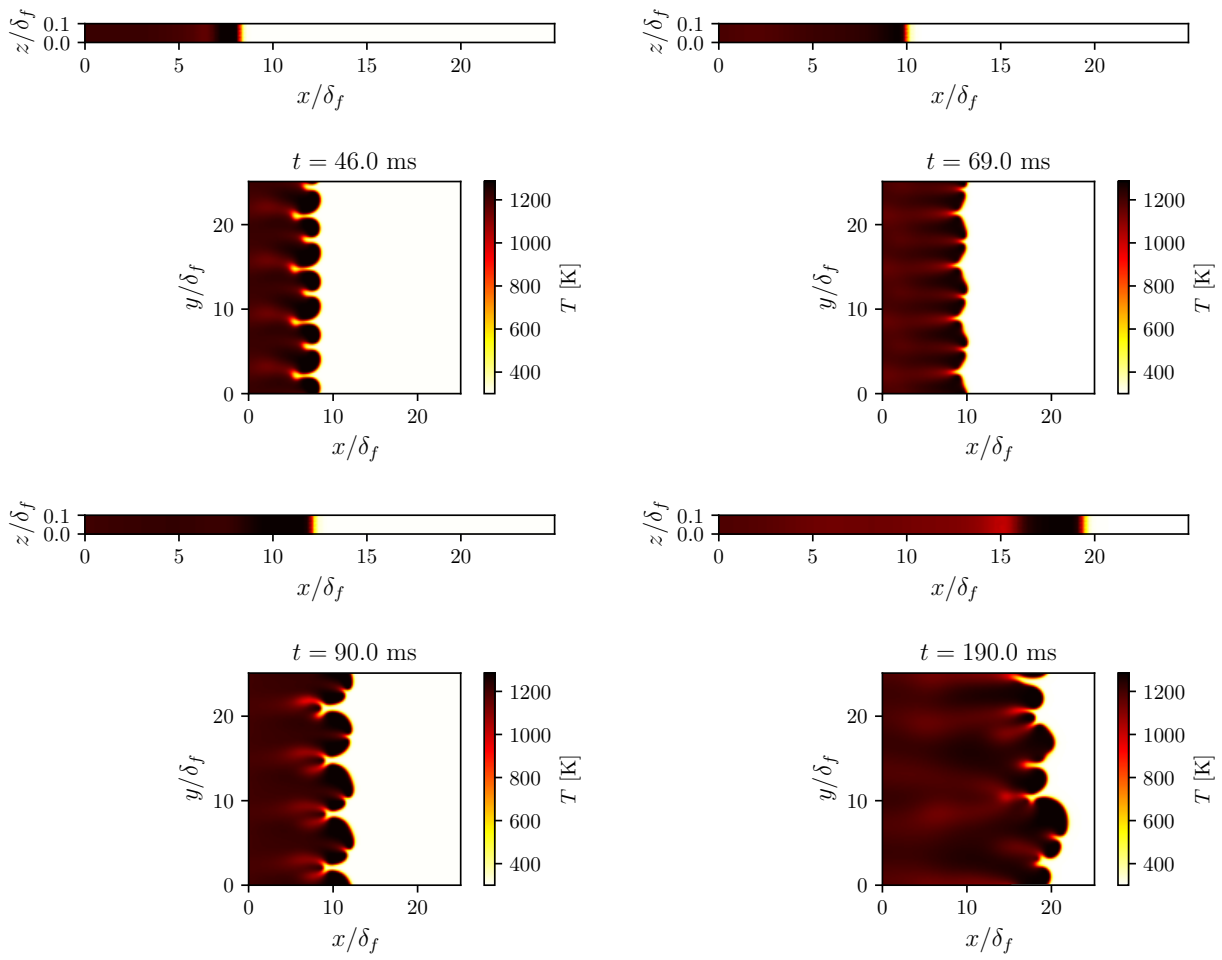

Figure 3: Temperature fields for $h = 0.1\delta_f$. Each time instance is composed of two views: zx-plane at $L_y = y_{\min}$ (top) and xy-plane at $L_z = z_{\max}$ (bottom).

breaks the aforementioned uniformity leading to additional length scales present in the flame topology. The resemblance of the latter temperature field with the so-called *viscous fingering* obtained during drainage processes through porous media is striking [27]. This instability typically occurs for situations in which a less viscous fluid displaces another fluid whose viscosity is larger. In the opposite situation the interface is stable according to the classical experiments and theory of Saffman and Taylor [28]. Joulin and Sivashinsky [7] argue that the resistance-to-flow induced by frictional forces ahead of the flame is another source of instability; the latter effect being more pronounced for small values of h. The topology observed for $h = 0.1\delta_f$ is thus probably linked with this mechanism, in addition to thermal expansion and differential diffusion. Note that contrary to cold flows, in reacting flows it is difficult to isolate the effect of viscosity changes as it is always accompanied by burnt gases expansion.

Following the same methodology as for $h = 0.1\delta_f$, we show in Fig. 4 the flame topology at four instances during propagation for $h = 0.5\delta_f$. Slightly larger cells are observed, of about $6.25\delta_f$ on the $xy-$plane, however the splitting and merging dynamics is milder (see Fig. 4 at $t = 45 - 162$ ms) leading to significantly reduced consumption rates. An incipient curvature (concavity) along the $xz-$plane is visible at $t = 293$ ms together with formation of smaller cells ($\sim 3.85\delta_f$). As frictional forces are reduced compared to $h = 0.1\delta_f$, viscous fingering is expectedly less pronounced. Close inspection of the temperature fields in Figs. 3 and 4 at approximately the same times, $t = 46$ ms ($h = 0.1\delta_f$) and $t = 45$ ms

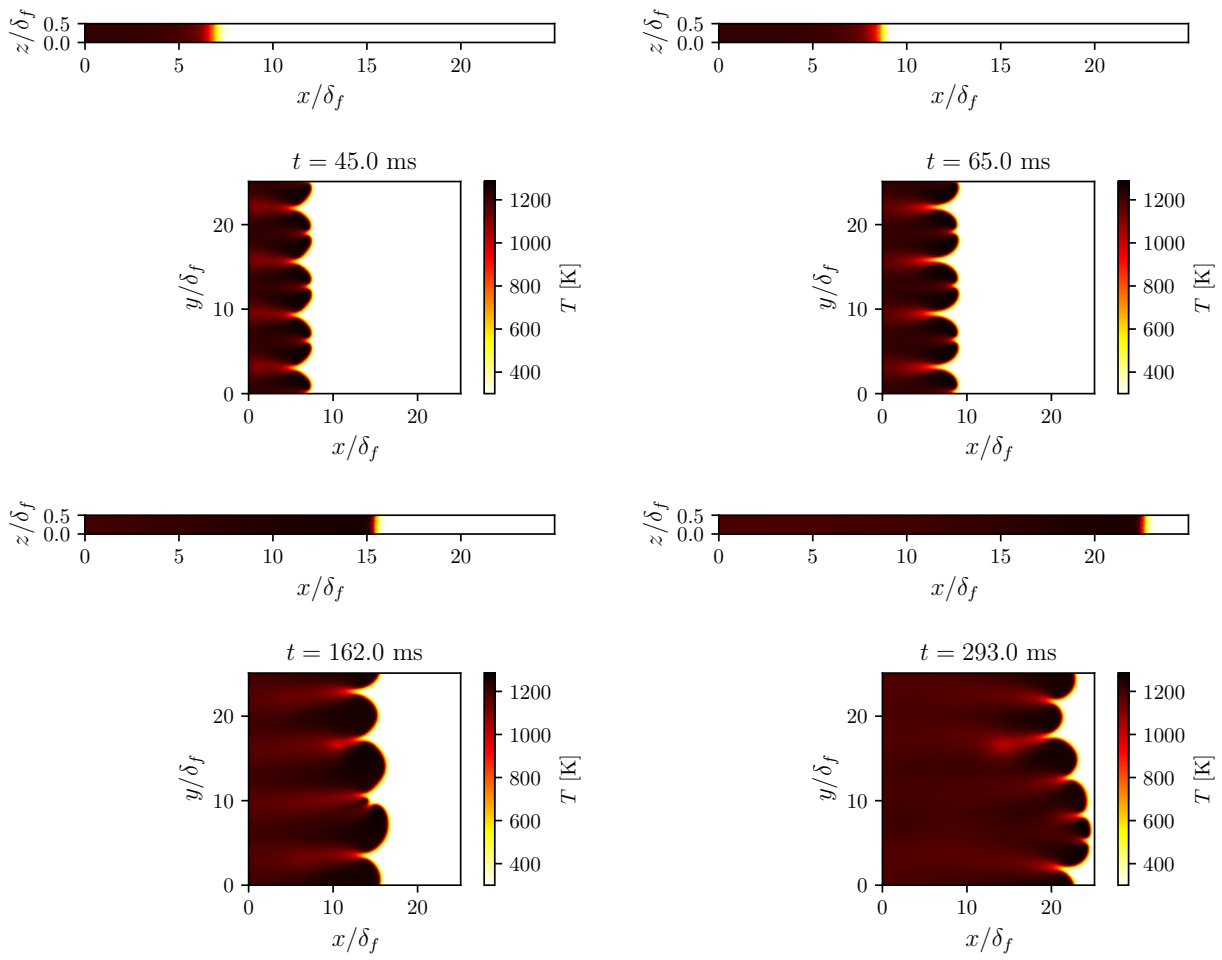

Figure 4: Temperature fields for $h = 0.5\delta_f$. Each time instance is composed of two views: zx-plane at $L_y = y_{\min}$ (top) and xy-plane at $L_z = z_{\max}$ (bottom).

($h = 0.5\delta_f$) reveals how the flame topologies are affected by confinement at early stages of propagation.

A further increase in the distance between plates to $h = \delta_f$ leads to a completely different evolution as the curvature in $z-$direction starts to play a role in the flame dynamics. The flame topologies in Fig. 5 show distinct phases along the $xz-$plane: symmetric propagation at 15 ms; early signs of asymmetry at 45 ms, followed by transition to asymmetric propagation at 55 ms. The transition takes place gradually with the cells that propagate attached to the front wall sequentially detaching from it; the late stages of this transition process is visible at $t = 55$ ms showing two cells, at $y/\delta_f \sim 5$ and 12, still propagating attached to the front wall. At $t = 120$ ms fully asymmetric propagation is shown in which all cells are detached from the front wall. The symmetry breakdown along the xz-plane increases the fuel consumption rate showing an important feature of the 3D flame dynamics that the quasi-2D approximation would not be able to capture. This flame asymmetry was reported in [29] but for a slightly richer mixture ($\phi = 0.4$) and at values of h above 0.7 mm (i.e., $h/\delta_f > 1.03$ using its corresponding δ_f) indicating that the limit of applicability of the quasi-2D approximation may be equivalence ratio (ϕ) or lewis number (Le) dependant; we plan to investigate this in future. Note also the stark difference in the size, hence number of cells, admitted on the $xy-$plane compared to the previous cases ($1.56\delta_f$). Strong confinement seems to increase the characteristic size of the observed cells in the $xy-$plane clearly showing that this is a consequence of the resistance-to-flow alluded to earlier as this is the only mechanism that is

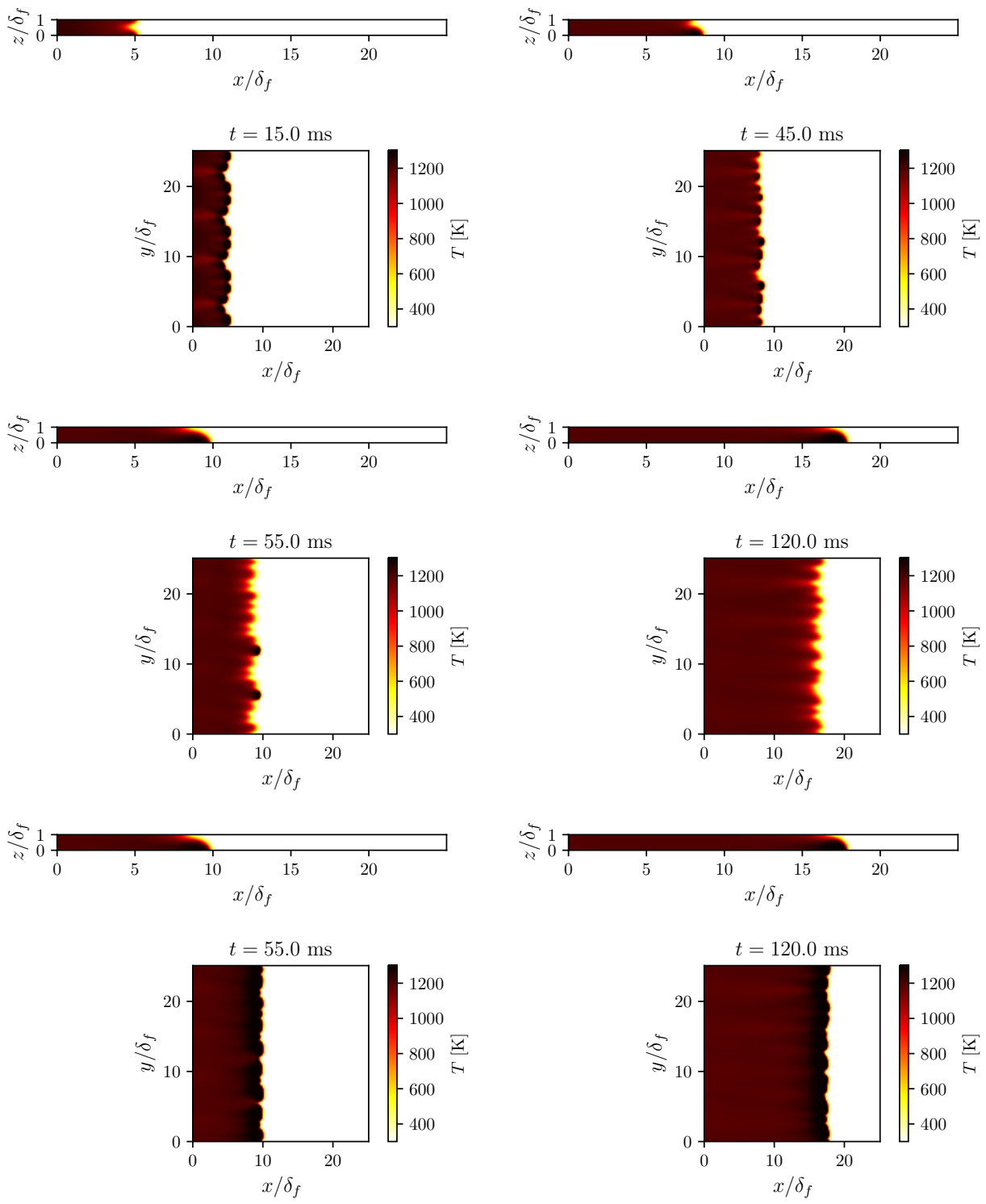

Figure 5: Temperature fields for $h = \delta_f$. Each time instance is composed of two views: zx-plane at $L_y = y_{\min}$ (top) and xy-plane at $L_z = z_{\max}$ (bottom). For t = 55 ms and 120 ms the xy-plane at $L_z = z_{\min}$ is also shown.

enhanced/suppressed for decreasing/increasing h.

The resemblance between the 3D numerical results shown in Fig. 3 with those of [9] and [14] is evident.

Following [30], these two studies demonstrated that in the limit $a = h/\delta_f \ll 1$, the flow field variables $\Psi = \{T, Y_k, p\}$ can be expanded around the small parameter a as $\Psi = \Psi_0 + a^2\Psi_1 + O(a^4)$. In this limit, the momentum equation (2) in z reduces to $\partial p/\partial z = 0$, in the first approximation, and the viscous dominant terms in the x and y momentum equations lead to a velocity profile that becomes parabolic in the z direction, i.e., $\mathbf{u} = \mathbf{u}(x, y; t)$, and proportional to the spatial pressure gradient ∇p through Eq. (6). Similarly, the leading order solution $O(a^{-2})$ for the temperature and species mass fraction reduces to $\partial T/\partial z = \partial Y_k/\partial z = 0$, reaching a uniform profile $T = T(x, y; t)$ and $Y_k = Y_k(x, y; t)$ in the transverse coordinate z after imposing the boundary conditions at the walls. An identical behavior is observed in the 3D computations shown above in Fig. 3 for $h = 0.1\delta_f$, in clear contrast with the fields displayed in Fig. 5 for $h = \delta_f$. As mentioned above, the value of the parameter a below which the asymptotic approximation is valid is thus likely to be modified by the diffusion properties of the mixture considered, i.e., lean mixtures vs. near-stoichiometric or rich mixtures.

4. CONCLUSION

Flames propagating in confined geometries are exposed to additional hydrodynamic instability mechanisms associated with the frictional forces of the burned gas flow. To determine the validity of the limit $h/\delta_f \ll 1$ explored earlier within the quasi-2D approximation [9, 11, 14], 3D simulations with detailed chemistry and transport were performed. The effect of h on the propagation dynamics of a lean H_2-air flame ($\phi = 0.3$) in a Hele-Shaw cell was examined for $h = 0.1\delta_f$, $h = 0.5\delta_f$ and $h = \delta_f$. Results show that the flame topology differs in each case. For $h = 0.1\delta_f$ the propagation speed has low frequency/high amplitude oscillations ranging between $5 \leq S_T/S_L \leq 11$, showing similarities with the quasi-2D approximation. The flame topology resembles that of a typical *viscous fingering* with characteristic cell sizes of about $2.5 - 5\delta_f$ in the xy-plane. For $h = 0.5\delta_f$ the propagation speed is lower attaining values of $S_T/S_L \sim 5.5 - 6$ close to the end wall. The topology is similar to the case $h = 0.1\delta_f$ but with larger cells ($6.25\delta_f$). For $h = \delta_f$ the instability associated to differential diffusion breaks the symmetry of the flame in the xz-plane. This mechanism introduces a very different behavior in the consumption rate history showing a steady propagation of about $S_T/S_L \sim 10$ with high frequency/low amplitude oscillations. The cell sizes are reduced drastically to about $1.56\delta_f$. Our results seem to indicate that strong confinement increases the characteristic size of the observed cells in the xy-plane as well as the cell splitting/merging dynamics; the quasi-2D approximation for the mixture considered seems to break down for $h > 0.1\delta_f$. Future work will include the implementation of the quasi-2D formulation within the OpenFOAM framework to allow for fair/direct quantitative comparison of its limits of validity as a function of ϕ, as well as the exploration of the flame dynamics for non-adiabatic walls which may lead to capturing isolated flame cells as those observed in [15].

ACKNOWLEDGMENTS

This work was carried out in the Detonation Team of the Institut Pprime UPR 3346 CNRS, and used the supercomputer facilities of the Mésocentre de Calcul de Poitou Charentes. The contributions of Karthik Thyagarajan to the implementation of the Cantera class and AMR capabilities during his 2019 summer internship at Pprime are gratefully acknowledged.

REFERENCES

1. M. Matalon. Flame dynamics. *Proceedings of the Combustion Institute*, 32(1):57–82, 2009.
2. M. Sánchez-Sanz, D. Fernández-Galisteo, and V.N. Kurdyumov. Effect of the equivalence ratio, Damköhler number, Lewis number and heat release on the stability of laminar premixed flames in microchannels. *Combust. Flame*, 161:1282–1293, 2014.
3. B. Radisson, B. Denet, and C. Almarcha. Nonlinear dynamics of premixed flames: from deterministic stages to stochastic influence. *Journal of Fluid Mechanics*, 903, 2020.
4. M. Tayyab, B. Radisson, C. Almarcha, B. Denet, and P. Boivin. Experimental and numerical lattice-boltzmann investigation of the Darrieus–Landau instability. *Combustion and Flame*, 221:103–109, 2020.
5. G. Searby. Acoustic instability in premixed flames. *Combustion Science and Technology*, 81(4-6):221–231, 1992.
6. M. Sánchez-Sanz. Premixed flame extinction in narrow channels with and without heat recirculation. *Combust. Flame*, 159:3158–3167, 2012.
7. G Joulin and G Sivashinsky. Influence of momentum and heat losses on the large-scale stability of quasi-2D premixed flames. *Combustion Science and Technology*, 98(1-3):11–23, 1994.
8. S.H. Kang, S.W. Baek, and H.G. Im. Effects of heat and momentum losses on the stability of premixed flames in a narrow channel. *Combustion Theory and Modelling*, 10(4):659–681, 2006.
9. D. Fernández-Galisteo, V.N. Kurdyumov, and P.D. Ronney. Analysis of premixed flame propagation between two closely-spaced parallel plates. *Combustion and Flame*, 190:133–145, 2018.
10. F. Veiga-López, D. Martínez-Ruiz, E. Fernández-Tarrazo, and M. Sánchez-Sanz. Experimental analysis of oscillatory premixed flames in a hele-shaw cell propagating towards a closed end. *Combustion and Flame*, 201:1–11, 2019.
11. D. Fernández-Galisteo and V. N. Kurdyumov. Impact of the gravity field on stability of premixed flames propagating between two closely spaced parallel plates. *Proceedings of The Combustion Institute*, 37:1937–1943, 2019.
12. L.R. Boeck, J. Melguizo-Gavilanes, and J.E. Shepherd. Hot surface ignition dynamics in premixed hydrogen–air near the lean flammability limit. *Combustion and Flame*, 210:467–478, 2019.
13. F. Veiga-López, D. Martínez-Ruiz, M. Kuznetsov, and M. Sánchez-Sanz. Thermoacoustic analysis of lean premixed hydrogen flames in narrow vertical channels. *Fuel*, 278:118212, 2020.
14. D. Martínez-Ruiz, F. Veiga-López, D. Fernández-Galisteo, V.N. Kurdyumov, and M. Sánchez-Sanz. The role of conductive heat losses on the formation of isolated flame cells in hele-shaw chambers. *Combustion and Flame*, 209:187–199, 2019.
15. F. Veiga-López, M. Kuznetsov, D. Martínez-Ruiz, E. Fernández-Tarrazo, J. Grune, and M. Sánchez-Sanz. Unexpected propagation of ultra-lean hydrogen flames in narrow gaps. *Physical review letters*, 124(17):174501, 2020.
16. D. Martínez-Ruiz, F. Veiga-López, and M. Sánchez-Sanz. Premixed-flame oscillations in narrow channels. *Physical Review Fluids*, 4(10):100503, 2019.
17. T. Poinsot and D. Veynante. *Theoretical and Numerical Combustion*. Edwards, 2005.
18. H. G. Weller, G. Tabor, H. Jasak, and C. Fureby. A tensorial approach to computational continuum mechanics using object-oriented techniques. *Computers in Physics*, 12(6):620–631, 1998.
19. J. Melguizo-Gavilanes, L.R. Boeck, R. Mével, and J.E. Shepherd. Hot surface ignition of stoichiometric hydrogen-air mixtures. *International Journal of Hydrogen Energy*, 2016.
20. J. Melguizo-Gavilanes, A. Nové-Josserand, S. Coronel, R. Mével, and J.E. Shepherd. Hot surface ignition of n-hexane mixtures using simplified kinetics. *Combustion Science and Technology*, 2016.
21. J. Melguizo-Gavilanes, R. Mével, S. Coronel, and J.E. Shepherd. Effects of differential diffusion on ignition of stoichiometric hydrogen-air by moving hot spheres. *Proceedings of the Combustion Institute*, 2016.
22. R. Mével, U. Niedzielska, J. Melguizo-Gavilanes, S. Coronel, and J.E. Shepherd. Chemical kinetics of ignition of *n*-hexane by a moving hot sphere. *Combustion Science and Technology*, 2016.
23. J. Melguizo-Gavilanes, P.A. Boettcher, R. Mével, and J.E. Shepherd. Numerical study of the transition between slow reaction and ignition in a cylindrical vessel. *Combustion and Flame*, 204:116–136, 2019.
24. D.G. Goodwin, H.K. Moffat, and R.L. Speth. Cantera: An object-oriented software toolkit for chemical kinetics, thermodynamics, and transport processes, 2009.
25. R. Mével, S. Javoy, F. Lafosse, N. Chaumeix, G. Dupré, and C. E. Paillard. Hydrogen-nitrous oxide delay time: shock tube experimental study and kinetic modelling. *Proceedings of The Combustion Institute*, 32:359–366, 2009.
26. R. Mével, S. Javoy, and G. Dupré. A chemical kinetic study of the oxidation of silane by nitrous oxide, nitric oxide and oxygen. *Proceedings of The Combustion Institute*, 33:485–492, 2011.
27. G.M. Homsy. Viscous fingering in porous media. *Annual review of fluid mechanics*, 19(1):271–311, 1987.
28. P.G. Saffman and G.I. Taylor. The penetration of a fluid into a porous medium or hele-shaw cell containing a more viscous liquid. *Proceedings of the Royal Society of London. Series A. Mathematical and Physical Sciences*, 245:312–329, 1958.
29. C. Jiménez, D. Fernández Galisteo, and V.N. Kurdyumov. DNS study of the propagation and flashback conditions of lean hydrogen-air flames in narrow channels: Symmetric and non-symmetric solutions. *International Journal of Hydrogen Energy*, 40:12541–12549, 2015.
30. V.N. Kurdyumov and M. Matalon. Flame acceleration in long narrow open channels. *Proceedings of The Combustion Institute*, 34:865–872, 2013.